Distinctive In-plane Cleavage Behaviors of Two-Dimensional Layered Materials

Yao Guo,[†] Chunru Liu,[†] Qifang Yin,[⊥] Chengrong Wei,[||] Shenghuang Lin,[†] Tim B. Hoffman,[#] Yuda Zhao,[†] J. H. Edgar,[#] Qing Chen,[§] Shu Ping Lau,[†] Junfeng Dai,[||] Haimin Yao,[⊥] H. –S. Philip Wong,[†‡] and Yang Chai[†*]*

[†] Department of Applied Physics, The Hong Kong Polytechnic University, Hung Hom, Kowloon, Hong Kong, People's Republic of China.

[‡] Department of Electrical Engineering, Stanford University, California 94305, USA

[§] Key Laboratory for the Physics and Chemistry of Nanodevices, Department of Electronics, Peking University, Beijing 100871, People's Republic of China

[⊥] Department of Mechanical Engineering, the Hong Kong Polytechnic University, Hung Hom, Kowloon, Hong Kong, People's Republic of China

[||] Physics Department, Southern University of Science and Technology, Shenzhen 518055, People's Republic of China

[#] Department of Chemical Engineering, Kansas State University, Manhattan, Kansas 66506, USA

Abstract- Mechanical exfoliation from bulk layered crystal is widely used for preparing two-dimensional (2D) layered materials, which involves not only out-of-plane interlayer cleavage but also in-plane fracture. Through a statistical analysis on the exfoliated 2D flakes, we reveal the in-plane cleavage behaviors of 6 representative layered materials, including graphene, *h*-BN, 2H phase MoS_2, 1T phase PtS_2, $FePS_3$ and black phosphorous. In addition to the well-known interlayer cleavage, these 2D layered materials show distinctive tendency to fracture along certain in-plane crystallography orientations. With theoretical modeling and analysis, these distinct in-plane cleavage behaviors can be understood as a result of the competition between the release of the

elasticity energy and the increase of the surface energy during the fracture process. More importantly, these in-plane cleavage behaviors provide a fast and non-invasive method using optical microscopy to identify the lattice direction of mechanical exfoliated 2D layered materials.

Keywords: two-dimensional layered materials, graphene, transition metal dichalcogenides, in-plane cleavage, anisotropy

TOC graphic:

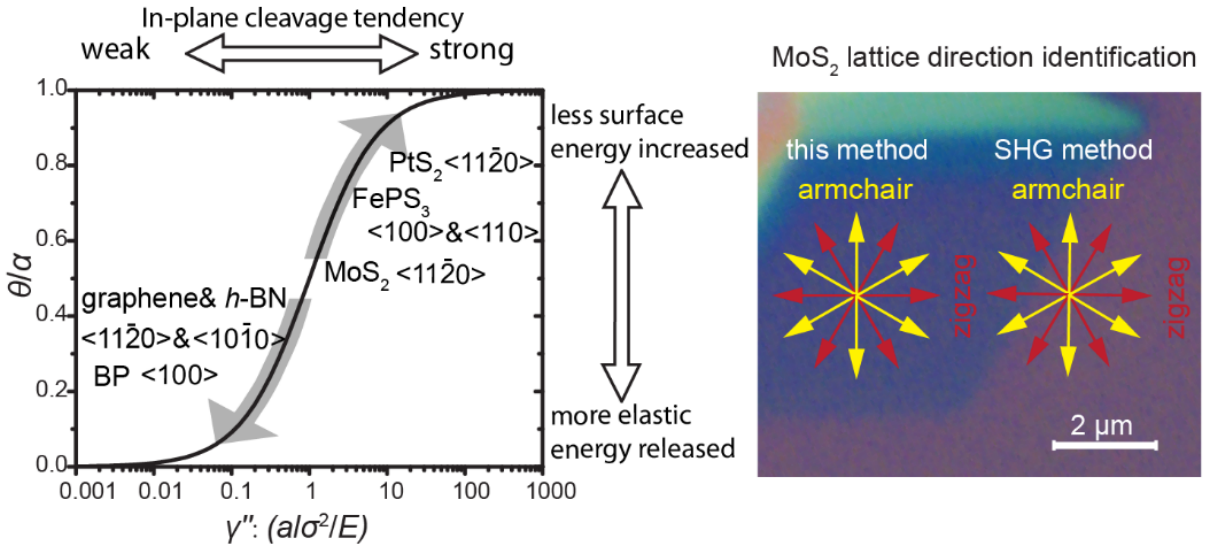

Layered materials usually have weak van der Waals out-of-plane interaction and strongly covalent in-plane bonds. This characteristic allows layered materials to be mechanically exfoliated into two-dimensional (2D) atomically thin layers, which have attracted intensive researches in recent years because of their unique physical properties.[1-6] With mechanical exfoliation, the out-of-plane cleavage reduces the thickness of layered materials down to single- or few-atoms limit, while the in-plane fracture defines the edge profile, which significantly affects physical and catalytic properties of 2D layered materials.[7-17] In addition to the interlayer interactions of these 2D layered materials, their in-plane mechanical properties, such as Young's modules, fracture strengths as well as their in-plane fracture behaviors,[18-23] are also of great of interest. These fundamental studies are important for understanding the performance and reliability of flexible devices and nanoscale resonators based on these 2D layered materials. [24-30] However, there have been few systematic studies elaborating the in-plane fracture behaviors of the 2D layered materials, including graphene, *h*-BN, transition metal dichalcogenides (TMDCs), black phosphorous (BP) and ternary 2D materials, such as $FePS_3$.

Recent studies have shown that the physical properties of 2D materials are highly in-plane anisotropic, such as piezoelectric effect, charge carrier mobility, vibrational modes, optical properties, mechanical properties, and strain induced band-structure modulations. [31-47] Identifying the crystallography orientations of 2D materials is essential for studying the anisotropic properties. There have been a few methods for the crystallography orientations identification of 2D materials, such as transmission electron microscopy (TEM),[48] second harmonic generation (SHG),[45, 46] polarized infrared absorption, [40] and Raman spectrum.[37, 43, 47] However, these methods require costly facilities, time-consuming process, and the long-time electron or photo beam irradiation that possibly induces damages to the materials. Therefore, it is imperative to develop a fast and non-

invasive method for identifying crystallography orientations of 2D layered materials. Optical microscopy has already been adopted for fast identification of the layer number, the grain boundaries and point defects of 2D materials. [49-52]

In this work, we conduct a statistical analysis to reveal the in-plane fracture behaviors of six types of representative 2D layered materials (graphene, *h*-BN, 2H MoS_2, 1T PtS_2, $FePS_3$ and BP). These 2D layered materials show distinct tendency to cleave along specific preferred crystallography orientations. A theoretical model is built to reveal the kinetics of the in-plane cleavage behaviors of the 2D layered materials. Based on our understanding of in-plane cleavage behaviors, we present a fast and non-invasive method to identify the lattice direction of the 2D layered materials through optical microscopy.

Results and discussions

Distinctive cleavage behaviors of 2D materials. Layered materials were exfoliated onto the Si/SiO_2 substrate using the mechanical exfoliation method. Figure 1a and 1b show representative optical images of the cleaved graphene and *h*-BN flakes,[53] respectively. The edges of the exfoliated flakes resulted from the in-plane fracture during the mechanical exfoliation, providing possible clues for analyzing the in-plane fracture behaviors of the layered materials. The exfoliated 2D flakes show straight regular edges (labelled with black line) and curved irregular edges (labeled with white dot line). For each exfoliated flake, the angles between two straight edges (called as "edge angle" in this work) are measured and counted. A total of 376 edge angles were counted from 150 graphene flakes, and the statistical distributions is shown in Figure 1c. The edge angles of graphene exhibit moderate tendency to form 0°, 30°, 60° and 90°. Exfoliated *h*-BN flakes share similar statistical edge angle distribution to that of graphene, as shown in Figure 1d. The tight edge angle distribution indicates that the graphene and *h*-BN tend to fractures along certain in-plane

crystallographic orientations. As shown in Figure 1e and 1f, graphene and *h*-BN are layered materials with AB stacked hexagonal atomic layers. <$10\bar{1}0$> and <$11\bar{2}0$> are the two low-index crystallographic orientation families, along which the fracture process results in armchair and zigzag edges, respectively. The angle between a zigzag edge and another zigzag edge of a graphene or *h*-BN flake is 0° or 60°, the angle between an armchair edge and another armchair edge of a graphene or *h*-BN flake is also 0° or 60°, and the angle between a zigzag edge and an armchair edge of a flake is 30° or 90°. The relatively abundance of the edge angles at 0°, 30°, 60° and 90° indicates that graphene and *h*-BN flakes tend to fracture along both <$10\bar{1}0$> and <$11\bar{2}0$> orientations, forming zigzag-zigzag, armchair-armchair, and zigzag-armchair edge angles. To validate this conclusion, we transfer mechanically exfoliated graphene and *h*-BN flakes to a TEM grid for crystallographic orientation identification. Figure 1g and 1h shows the TEM images and the selected area electron diffraction (SAED) patterns (inset) of the graphene and *h*-BN flakes, respectively. We can determine the crystallography orientation of the edge of the flake by comparing the TEM micrographs with the corresponding SAED patterns. The straight edges forming the angle of 90° or 30° are identified to be along the <$11\bar{2}0$> (zigzag edge) and <$10\bar{1}0$> (armchair edge) respectively, as shown in Figure 1g (graphene) and 1h (*h*-BN). These results confirm that graphene and *h*-BN do tend to fracture along both the <$10\bar{1}0$> and <$11\bar{2}0$> orientations, in good agreement with the inference from the statistical distribution of the edge angles observed from optical images.

The layered materials of 2H MoS_2, 1T PtS_2 and $FePS_3$ have hexagonal in-plane structure. Their out-of-plane stacking orders are “AB”, “AA” and “ABC” stacking, respectively. [54, 55] Figure 2a, 2b and 2c show the representative optical images of 2H MoS_2, 1T PtS_2 and $FePS_3$ flakes exfoliated onto the Si/SiO_2 substrate, respectively. Figure 2d, 2e and 2f show the angle distribution of the

straight edges of the same 2H MoS_2, 1T PtS_2 and $FePS_3$. Although 2H MoS_2, 1T PtS_2 and $FePS_3$ shares similar in-plane hexagonal structure to that of graphene and *h*-BN, their edge angles are predominantly around 0° and 60° instead of 0°, 30°, 60° and 90°. Using a similar analysis as above, this distinctive edge angle distribution suggests that 2H MoS_2, 1T PtS_2 and $FePS_3$ tend to form only armchair-armchair edge angles or zigzag-zigzag edge angles, rather than armchair-zigzag edge angles. To identify the crystallography orientations of the edges, we transfer the exfoliated 2H MoS_2, 1T PtS_2 and $FePS_3$ flakes onto a TEM grid for further identification, as shown in Figure 2g, 2h and 2i, respectively. By correlating the TEM image of the flakes and the corresponding SAED patterns, we can identify the crystallography orientations of 2H MoS_2, 1T PtS_2 and $FePS_3$ flakes that form the edge angle of 60°. For the 2H MoS_2 and 1T PtS_2, the edges forming the angle of 60° are along the $<11\bar{2}0>$ orientation; for $FePS_3$, where the three-fold rotation symmetry of ABC stacking is broken,[56] the edges forming the angle of 60° are along <100> and <110> orientations.

BP is one kind of orthorhombic layered materials with highly anisotropy properties such as Raman scattering, infrared absorption and electrical conductivity.[19, 35, 36, 40] BP flakes were exfoliated onto the Si/SiO_2 substrate, as shown in Figure 3a. In the same manner, we collected statistics of the edge angles of the exfoliated BP flakes. As shown in Figure 3b, the distribution of the edge angles of BP does not exhibit strong tendency as that of TMDCs. However, we notice that there are a few elongated BP flakes with two parallel edges, which form the angle of about 0°, as shown in the inset (and more in Figure S1). The three low-index crystallography orientations of BP, <100>, <010> and <110>, are schematically described in Figure 3c. These few elongated flakes with parallel edges are possibly due to the weak tendency that BP fracture along one certain orientation. To distinguish the orientation of the edges, we conducted angle-resolved polarized

Raman spectrum measurement on 9 elongated flakes with parallel edges. For 6 of the measured elongated BP flakes, the parallel edges are along the <100> orientation. When the polarization direction of the stimulating laser is parallel with the edge, the peak ratio of A_g^1/A_g^2 reaches a minimum; when the polarization direction of the simulating laser is perpendicular to the edges, A_g^1/A_g^2 reaches a maximum, as shown in Figure 3d. This feature demonstrates that BP do have a weak tendency to fracture along the <100> orientation, resulting in the few more edge angles concentrating around 0°, which is in good consistent with the previous study that it is easier to fracture BP flakes along the <100> orientation.[19]

Cleavage is the tendency that crystalline materials split along definite orientations with atomically smooth fracture surfaces. With the statistical results of the edge angle distributions and the experimental characterizations show0-n above, we have revealed that layered materials tend to cleave along certain in-plane crystallography orientations. In addition to the edge angle distributions, we also collected statistical distribution of the length of the straight edges (as marked with the black solid lines in the optical images, see Figure 1a, 1b, 2a, 2b, 2c, 3a) and of the curved edges (as marked with the white dotted lines in the images, see Figure 1a, 1b, 2a, 2b, 2c, 3a), as shown in Figure 4. The length distributions are different for each layered material. Basically, the trend is in accordance with the spread of the angle distributions. The tighter the edge angle distributions are (see Figure 1c, 1d, 2d, 2e, 2f, 3b), the larger the length proportion of the straight edges is (see Figure 4), which indicates the tendency of in-plane cleavage is more strong. As summarized in Table I, BP shows relatively weak tendency to cleave along the orientation of <100>, graphene and *h*-BN shows moderate tendency to cleave along the orientation of $<10\bar{1}0>$ and $<11\bar{2}0>$; 2H phase MoS_2 shows strong tendency to cleave along the orientation of $<11\bar{2}0>$;

$FePS_3$ shows stronger tendency to cleave along the orientation of <100> and <110>; and 1T phase PtS_2 shows the strongest tendency to cleave along the orientation of $<11\bar{2}0>$.

Theoretical modeling. The distinctive in-plane fracture behaviors of 2D materials can be understood through an analysis of the change of the overall system energy during the fracture process. The change in overall system energy is determined by the competition between the reduction of elastic energy ($\triangle U$) and the increase of the surface energy ($\triangle E$). For the elastic energy, when in-plane strain is applied to an intact 2D materials flake with the thickness of t and the area of S, the elastic energy (U_0) stored in the flake can be described according to Equation (1)

$$U_0 = \frac{tS\sigma^2}{2E} \tag{1}$$

where E is the Young's modulus, σ is the stress raised by the strain. Figure 5a shows a fracturing flake in the presence of a crack. The crack results in a redistribution of the stress around the crack. The stress aside the crack is released, and the stress is concentrated around the tip of the crack. As a result, the overall elastic energy U is decreased by ΔU, which can be calculated by the integration,

$$U = \iint \frac{t\sigma_{xy}^2}{2E} dxdy = U_0 - \Delta U \tag{2}$$

where σ_{xy} is the stress distribution as a function of position. According to Griffith's theory, the decrease of elastic energy ΔU motivates the propagation of the crack.[57] On the other hand, the crack propagation is prevented by the increased surface energy $\triangle E$. The crack introduces extra fractured surfaces at the edge, raising the total energy by

$$\Delta E = 2tl\gamma \tag{3}$$

where γ is the surface energy per area, l is the length of the crack, and $2tl$ is the area of the newly created surface.

The decrease of elastic energy (ΔU) and the increase of surface energy (ΔE) are both dependent on the direction of the crack. We define θ as the angle between the crack direction and that perpendicular to the stress. For example, Figure 5a shows the simulated stress distribution of an in-plane stressed 10 μm × 10 μm × 0.1 μm flake with the crack of θ =15° using finite element model. The total elastic energy is integrated according to equation (2). To obtain $\Delta U(\theta)$, we simulated the stress distribution and elastic energy $U(\theta)$ of stressed flakes with the crack along θ=0, 5°, 10°…80°, and an intact flake (see Figure S2). As labelled by black solid squares in Figure 5b, $\Delta U(\theta)$ is well fitted with

$$\Delta U(\theta) = a\mathrm{t}\cos^2\theta l^2\sigma^2/E \quad (4)$$

The simulated coefficient a is 1.41, which is close to Griffith's estimation of a=π/2 (see Figure S3). When θ is small, we have

$$\Delta U(\theta) = at(1-\theta^2)l^2\sigma^2/E \quad (5)$$

The energy release $\Delta U(\theta)$ reaches maximum when θ=0 and the crack propagates perpendicular to the direction of the tension direction. On the other hand, the surface energy $\Delta E(\theta)$ can be expressed as a Taylor's series according to Equation (6),

$$\Delta E(\theta) = 2\mathrm{t}l[\gamma(\alpha) + \gamma'(\theta-\alpha) + \frac{\gamma''}{2!}(\theta-\alpha)^2 + \frac{\gamma'''}{3!}(\theta-\alpha)^3 + \cdots] \quad (6)$$

where α is the angle along which the cracked interface energy per area γ has a minimum (see Figure 5a), γ' is the first derivative versus θ, and γ'' is the second derivative versus θ, *etc.* As γ reaches minimum at θ=α, we have $\gamma' = 0$. Neglecting higher order terms, we have

$$\Delta E(\theta) = 2tl[\gamma(\alpha) + \frac{1}{2}\gamma''(\theta - \alpha)^2] \quad (7)$$

Thus, the overall decrease of the energy obtained with equation (5) and (7)

$$\Delta U(\theta) - \Delta E(\theta) = t[-\left(\frac{al^2\sigma^2}{E} + \gamma''l\right)\theta^2 + 2\gamma''\alpha l\theta - 2l\gamma(\alpha) - l\gamma''\alpha^2 + \frac{al^2\sigma^2}{E}] \quad (8)$$

is a binomial expression of θ. Suppose the crack propagates along the direction that reaches the maximum energy decrease $\Delta U(\theta, a) - \Delta E(\theta, a)$, we have $\theta = \gamma''\alpha/(al\sigma^2/E + \gamma'')$. The parameter γ'', which is related to the anisotropy of the materials, is the key factor that determines the fracture behavior. As Figure 5c shows, when γ'' is relatively small compared with $al\sigma^2/E$, we have θ approaching 0. The crack tends to propagate in a direction that is perpendicular to the tension direction so that the elastic energy releases at the fastest rate, and the fractured edges are less dependent on the crystallography orientation. When γ'' is relatively large, θ is approaching α, the crack tend to propagates along the crystallography orientations with the minimum surface energy, leaving cleaved edges with distinct edge angle distributions. The increasing tendency of fracture along the certain orientations of the above layered materials (*i.e.* <100> of BP; <$10\bar{1}0$> and <$11\bar{2}0$> of graphene and *h*-BN; <$11\bar{2}0$> of 2H MoS_2; <100> and <110> of $FePS_3$; and <$11\bar{2}0$> of 1T PtS_2) reveals the competition between the released elastic energy and the increase of surface energy, or specifically, the relationship between γ'' and $al\sigma^2/E$ of different layered materials.

Identification of crystallography orientations. The in-plane cleavage behavior along certain crystallography orientations offers a hint for fast crystallography orientations identification. Here we demonstrate that the crystallography orientations of the mechanically exfoliated 2D flakes can be identified by simply observing the morphology of the flakes using optical microscopy. Taking MoS_2 for example, the results presented above have shown that the MoS_2 flakes tend to cleave along the orientation of <$11\bar{2}0$>. Figure 6a shows a mechanically exfoliated monolayer MoS_2.

The presence of two straight edges forming the angle of 60° enables us to identify the lattice direction rapidly. The zigzag (<$11\bar{2}0$>) orientations of the monolayer MoS_2 flake are parallel to the edges (marked with red arrows), and the armchair (<$10\bar{1}0$>) orientations are perpendicular to the edges (marked with blue arrows). We corroborated the validity of the judgement with the commonly used SHG method.[45, 46] Figure 6b is the angle resolved SHG result of the same piece of MoS_2 flake in Figure 6a. These two methods identify lattice directions with good consistency, and the mismatch are less than 1° (~0.9°). Thus, we have provided a fast and non-invasive method for identifying the crystallography lattice direction of MoS_2, which can be used for further studies relating to the anisotropy properties and edge states. Our molecular dynamics simulation shows that the cleaved zigzag edges of MoS_2 are atomically smooth, while the edges along other directions are disordered with more dangling bonds, which increase the surface energy (Figure S4 and Movies SI-IV). It is noteworthy that not all the exfoliated MoS_2 flakes have straight edges with 60° angles. However, one can easily find those exfoliated MoS_2 flakes with more than a few straight edges, where the lattice directions can be perfectly identified with high precision and reliability (Figure S5).

We compare the pros and cons of this edge identification method with other methods commonly used for lattice direction identification. SHG method can be used for few layered MoS_2 only with odd layer numbers due to the requirement of symmetry, while this method by optical microscopy can be used for MoS_2 flakes without the limitation of layer number. SHG, infrared absorption, polarized Raman spectrum method and TEM requires costly facilities and time-consuming process, while identifying the edge orientations with optical microscopy images is easy and efficient. TEM induces damages to the sample with electron beam irradiation, while identifying the edge orientations with optical microscopy images is non-invasive to the sample. However, it should be

noted that this edge identification method is only applicable to layered 2D materials with a strong tendency to cleave along certain directions, such as 2H MoS_2, 1T PtS_2 and other analogous TMDCs, but not applicable to graphene and *h*-BN, whose in-plane cleavage happens both zigzag and armchair directions. In the above work of BP with polarized Raman spectrum measurement, we have demonstrated that BP flakes with elongated morphology tend to have lattice direction with <100> orientation parallel to the straight edges, but the reliability of this orientation identification still remains an open question because of its very weak tendency of in-plane cleavage.

Conclusion

In summary, we reveal the distinctive in-plane cleavage behaviors, including various preferred crystallography orientations tendencies of 6 presentative layered materials. Besides the Van der Waals' out-of-plane cleavage, we find that graphene and *h*-BN shows moderate tendency to cleave along the orientation of $<10\bar{1}0>$ and $<11\bar{2}0>$; 2H phase MoS_2 and 1T phase PtS_2 shows strong tendency to cleave along the orientation of $<11\bar{2}0>$; $FePS_3$ shows strong tendency to cleave along the orientation of <010> and <110>; and BP shows very weak tendency to cleave along the orientation of <100>. From the view of the system energy, these distinct in-plane cleavage behaviors are understood as the result of the competitions between the release of the elastic energy and increase of the surface energy of different layered materials. Based on this study, we demonstrate a fast and noninvasive method to identify the lattice direction of mechanical exfoliated layered materials flakes, which helps further studies on the rich anisotropy properties of layered materials.

Method:

Statistic of the characteristics of edges: graphene, *h*-BN, 2H MoS_2, 1T PtS_2, $FePS_3$ and BP flakes were exfoliated onto 300 nm SiO_2/Si substrates from bulk crystal by a commonly-used mechanical cleavage method. A piece of bulk crystal was separated by two sticky tapes (Nitto Tape) for a few times. The 2D materials with fresh surfaces were then attached onto the SiO_2 surface. After peeling off the tape, a number of 2D materials flakes were left onto the surface of SiO_2 substrate. The optical images of the 2D materials flakes were recorded by an optical microscope (LEICA DM1750M). Statistical analysis was made on the characteristics of the edges of these exfoliated flakes, including the total length of curved edges and straight edges, and the angle distributions of these straight edges.

Transition electron microscopy (TEM): The 2D materials flakes were firstly mechanically exfoliated onto Si/SiO_2 substrate. A TEM grid was put onto the surface of 2D flakes. KOH solution was then dropped onto the micro grids. The micro grids were separated from the substrate after a while. 2D materials flakes were attached onto the TEM grid. The micro grids were loaded into the TEM (JEOL JEM-2100F). Morphology images and the diffraction patterns of flakes were captured.

Polarized Raman spectroscopy: a 488 nm laser was used to excite Raman spectrum. A quarter-wave plate was used to modulate the polarization direction of exciting laser. The intensity of the Raman signal was recorded as the polarization direction of the exciting laser changes.

Second harmonic generation (SHG): a mode-locked Ti: sapphire laser at a wavelength of 810 nm with a pulse width of ~140 fs and a repetition rate of 80 MHz was used as excitation source. The laser pulse was focused to a spot size of ~1.1 μm on the sample by a 100x objective lens. The laser power irradiated on sample was 0.7mW. The intensity of the parallel second harmonic generation

signal was recorded by spectrometer equipped with a cooled charge-coupled device as the polarization direction of the exciting laser changes.

Molecular Dynamics simulations: Large-scale Atomic/Molecular Massively Parallel Simulator (LAMMPS)[58] package is used to conduct to Molecular Dynamics simulation. A 2H phase MoS_2 sheet with the size of about 40 nm × 40 nm is constructed, with the interactions between Mo and S atoms described by the Stillinger–Weber potential.[59] In order to simulate the dependence of the in-plane cleavage behaviors of MoS_2 on the crystallographic orientations, periodic boundary condition is applied on the AC direction for AC orientated case and ZZ direction for ZZ orientated case, respectively. In each case, a 2 nm long crack is first initiated on the edge of the sheet and then the sample is relaxed to its equilibrium state of almost zero stress. After the relaxation, a uniaxial tension is applied on the sheet in AC and ZZ directions, respectively, at a constant strain rate of 10^8 s^{-1}. All simulations are performed within NPT ensemble (constant number of atoms, constant pressure P=0 bar in the non-periodic directions and constant temperature T=10 K) and a constant time step of 1 fs. OVITO is used for visualization.[60]

AUTHOR INFORMATION

Corresponding Author: *E-mail: ychai@polyu.edu.hk

The authors declare no competing financial interest.

ACKNOWLEDGMENTS

We thank valuable discussions with Mr. Jiapei Shu, Mr. Zhibo Liu, Mr. Yi Wang and Dr. Xianlong Wei. This work was supported by the Research Grant Council of Hong Kong (Grant No.: PolyU 152145/15E) and the Hong Kong Polytechnic University (grant Nos.: 1-ZVDH, 1-ZVGH and G-SB53). Prof. Qing Chen acknowledges the financial support from the National Natural Science Foundation of China (Nos. 11374022, 61321001). Prof. Junfeng Dai acknowledges the financial support from Special Funds for the Development of Strategic Emerging Industries in Shenzhen (no. JCYJ20150630145302235).

Table I. Summary of distinct in-plane cleavage behaviors of six layered materials.

	Graphene	*h*-BN	2H-MoS_2	1T-PtS_2	$FePS_3$	BP
element	unitary	binary	binary	binary	ternary	unitary
in-plane structure	hexagonal	hexagonal	hexagonal	hexagonal	hexagonal	orthorhombic
staking order	AB	AB	AB	AA	ABC	AA
preferred orientation	<10$\bar{1}$0> <11$\bar{2}$0>	<10$\bar{1}$0> <11$\bar{2}$0>	<11$\bar{2}$0>	<11$\bar{2}$0>	<100> <110>	<100>
tendency (relative)	moderate	moderate	strong	strongest	stronger	weak

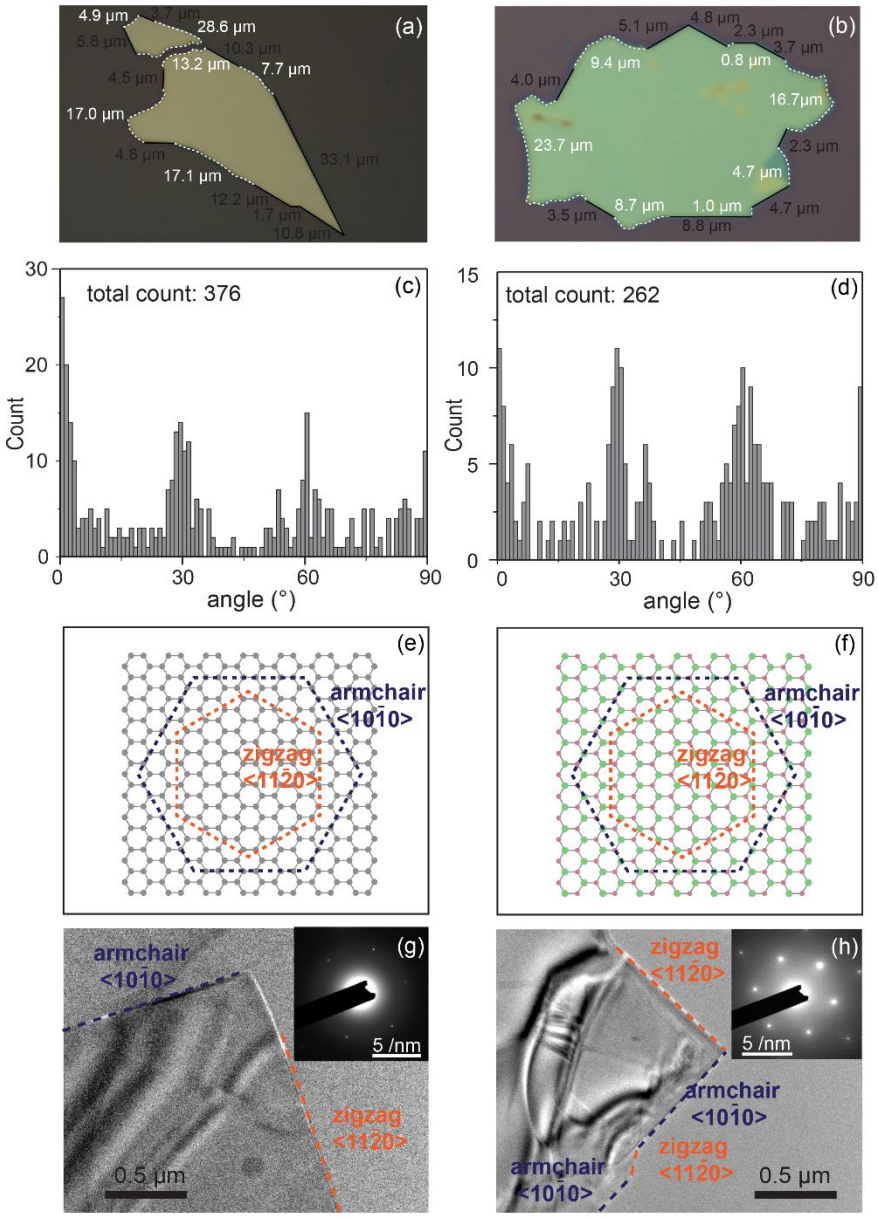

Figure 1. Optical microscope images of exfoliated graphene (a) and *h*-BN (b) flakes. Edge angle distributions of graphene (c) and *h*-BN (d) flakes. In-plane atomic structure of graphene (e) and *h*-BN (f) flakes. TEM morphology images and diffraction patterns of a graphene (g) and an *h*-BN (h) flake.

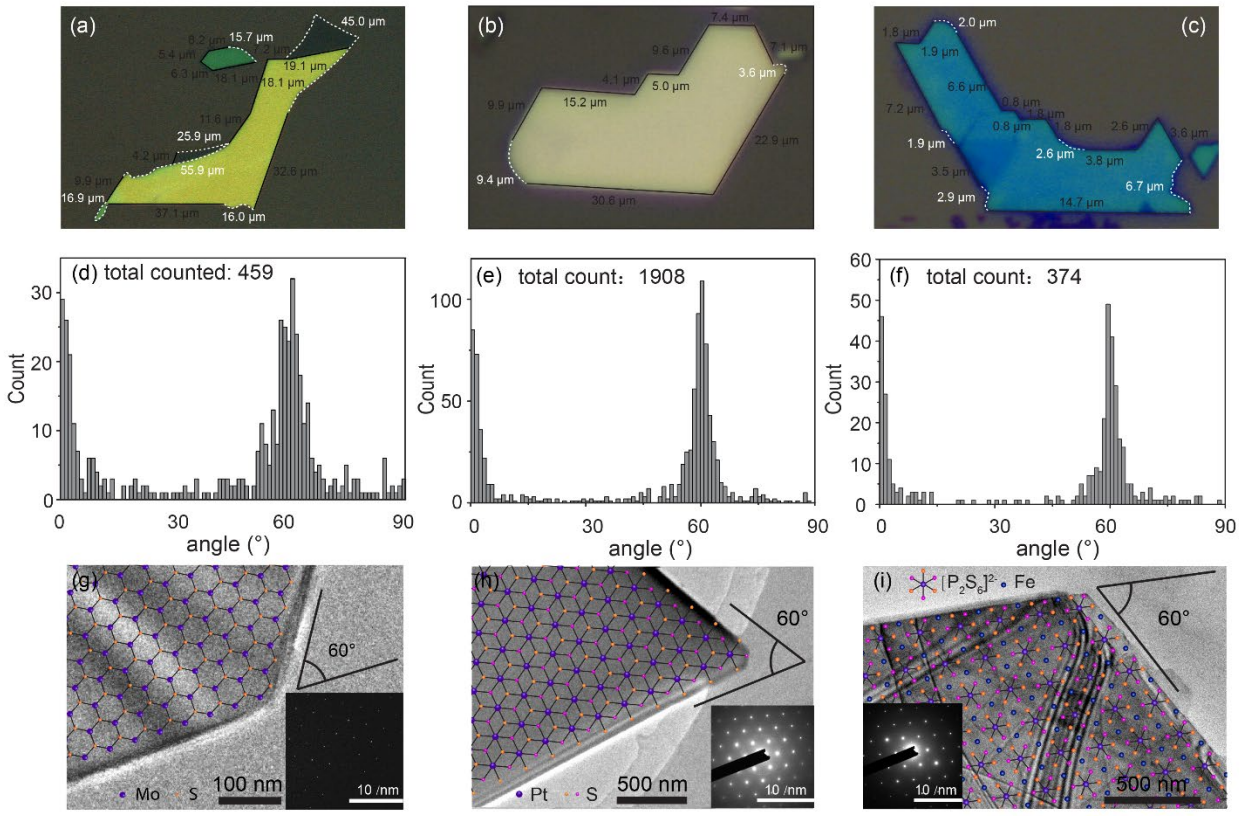

Figure 2. Optical microscope images of exfoliated 2H-MoS_2 (a), 1T-PtS_2 (b) and $FePS_3$ (c) flakes. Edge angle distributions of 2H-MoS_2 (d), 1T-PtS_2 (e) and $FePS_3$ (f) flakes. TEM morphology images, diffraction patterns and in-plane structures of a 2H-MoS_2 (g), an 1T-PtS_2 (h) and an $FePS_3$ (i) flake.

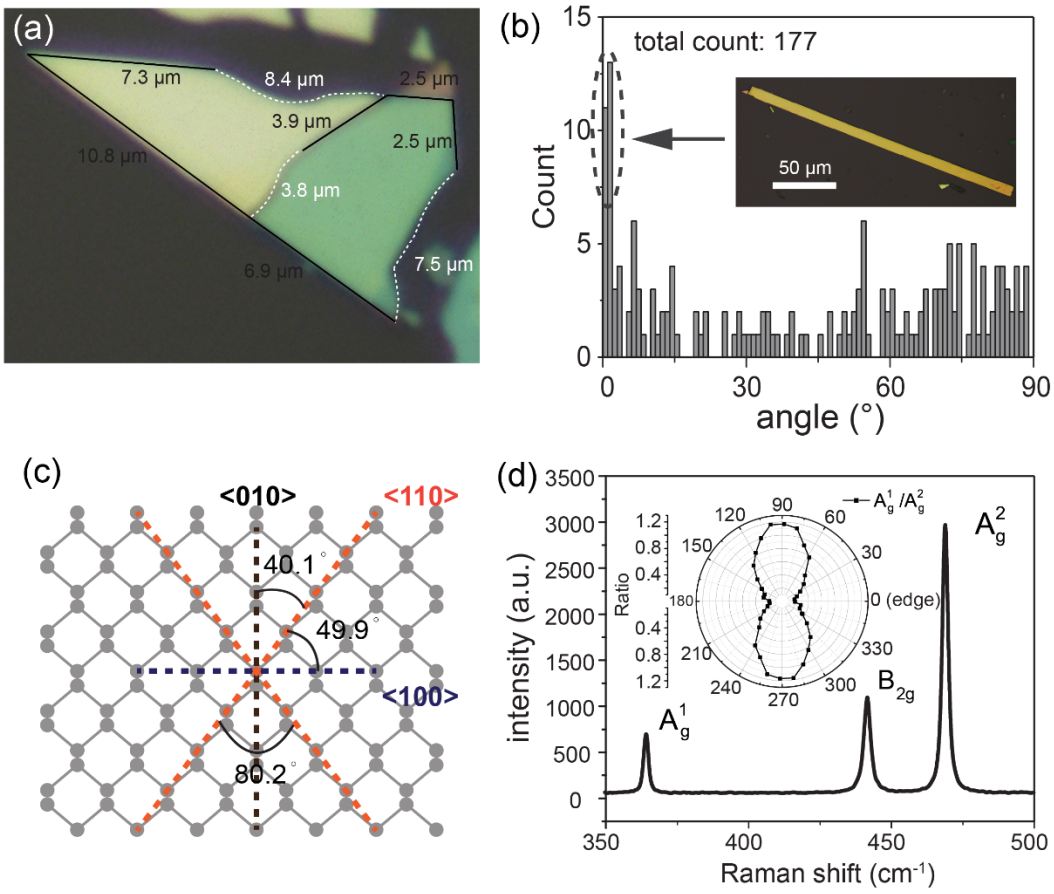

Figure 3. (a) Optical microscope images of exfoliated BP flakes. (b) Edge angle distributions of the BP flakes. (c) In-plane atomic structure of the BP flakes. (d) Raman spectrum of the BP flakes. The insert is the Raman polarization of the BP flakes. 0° corresponds to that the polarization direction of the exciting laser that is along the direction of the edge.

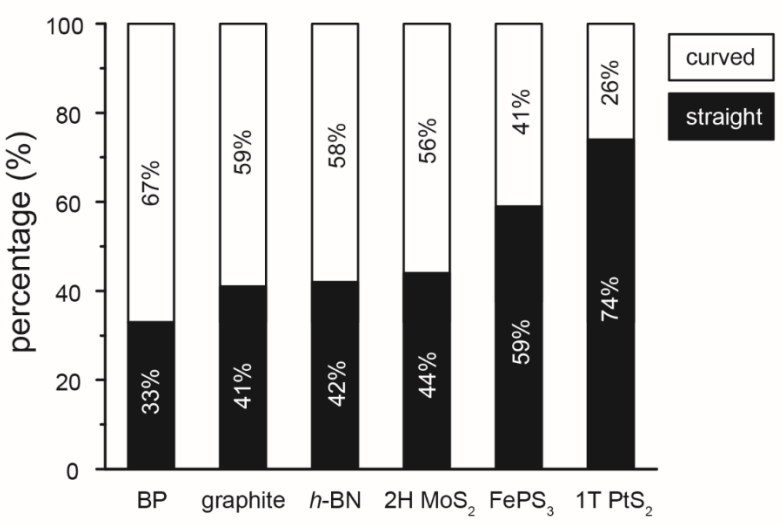

Figure 4. Length proportion of straight edges and curved edges of BP, graphene, h-BN, 2H MoS_2, $FePS_3$ and 1T PtS_2.

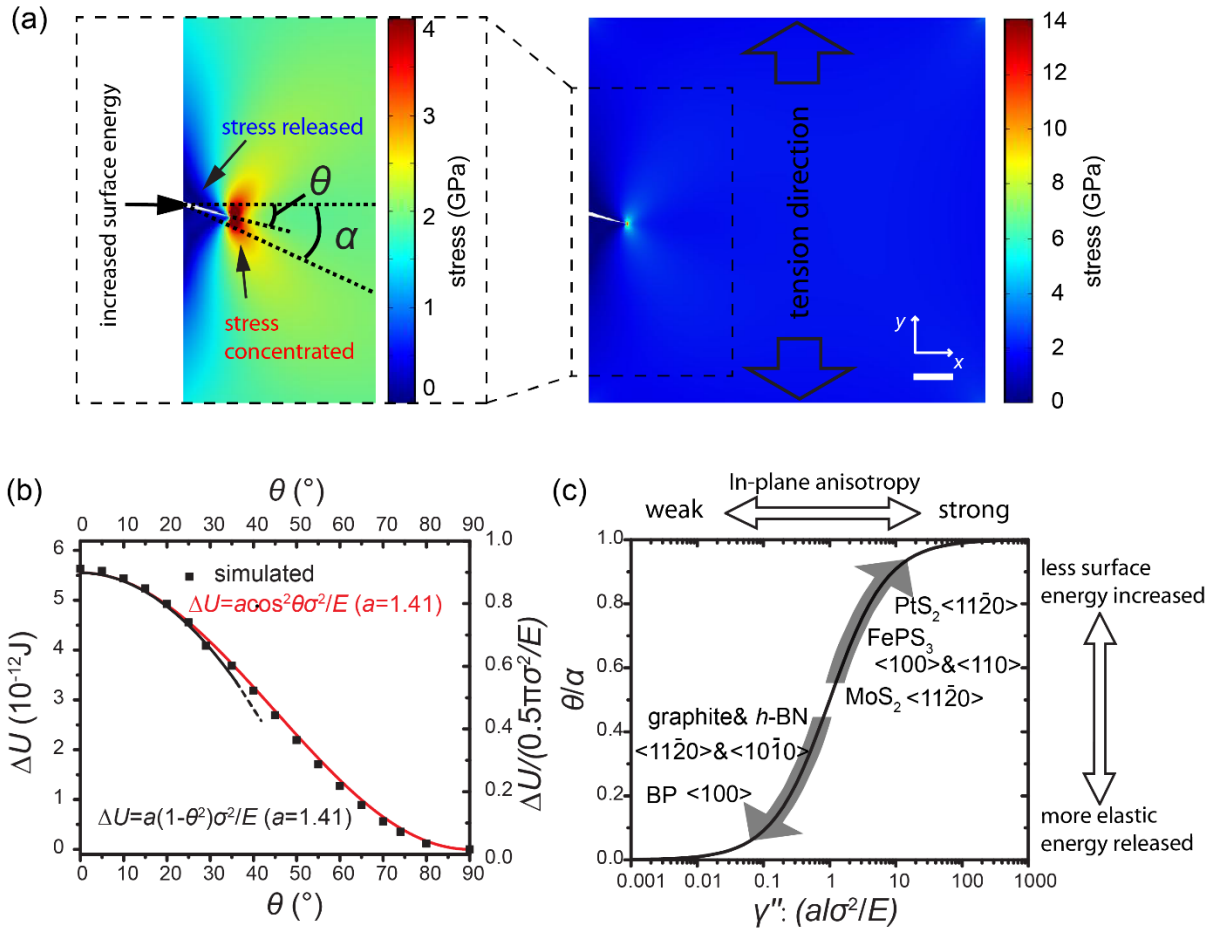

Figure 5. (a) Simulated stress distribution of a flake with a crack of θ=15°. θ is the angle between the crack direction and the stress-perpendicular direction. α is the angle along which the cracked interface energy per area γ has a minimum. The scale bar is 1 μm. (b) Simulated released elastic energy ΔU, which is well fitted with $\Delta U(\theta) = a\cos^2\theta l^2\sigma^2/E$ and $\Delta U(\theta) = at(1-\theta^2)l^2\sigma^2/E$ when θ is small. (c) The relationship of γ'' and $2al\sigma^2/E$, resulting in distinct in-plane cleavage behavior of different layered materials.

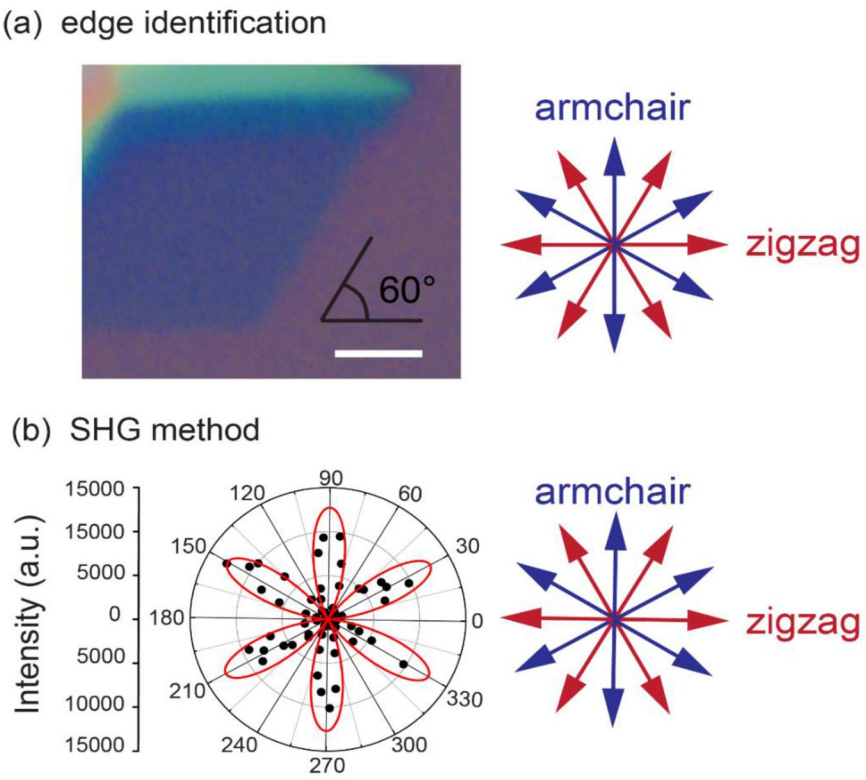

Figure 6. (a) Identifying the lattice direction of the MoS_2 flake via recognizing the cleaved edge with angle of 60°. The white scale bar is 2 μm. (b) Identifying the lattice direction of the same MoS_2 flake in (a) with SHG method. The mismatch of the orientations of these two method is 0.9°.

REFERENCES

1. Novoselov, K. S.; Geim, A. K.; Morozov, S. V.; Jiang, D.; Zhang, Y.; Dubonos, S. V.; Grigorieva, I. V.; Firsov, A. A. Electric Field Effect in Atomically Thin Carbon Films. *Science* **2004**, 306, 666-669.
2. Bhimanapati, G. R.; Lin, Z.; Meunier, V.; Jung, Y.; Cha, J.; Das, S.; Xiao, D.; Son, Y.; Strano, M. S.; Cooper, V. R., et al. Recent Advances in Two-Dimensional Materials Beyond Graphene. *ACS Nano* **2015**, 9, 11509-11539.
3. Xu, M.; Liang, T.; Shi, M.; Chen, H. Graphene-Like Two-Dimensional Materials. *Chem. Rev.* **2013**, 113, 3766-3798.
4. Huang, X.; Zeng, Z.; Zhang, H. Metal Dichalcogenide Nanosheets: Preparation, Properties and Applications. *Chem. Soc. Rev.* **2013**, 42, 1934-1946.
5. Yang, G.; Zhu, C.; Du, D.; Zhu, J.; Lin, Y. Graphene-Like Two-Dimensional Layered Nanomaterials: Applications in Biosensors and Nanomedicine. *Nanoscale* **2015**, 7, 14217-14231.
6. Geim, A. K. Graphene: Status and Prospects. *Science* **2009**, 324, 1530-1534.
7. Girit, Ç. Ö.; Meyer, J. C.; Erni, R.; Rossell, M. D.; Kisielowski, C.; Yang, L.; Park, C.-H.; Crommie, M. F.; Cohen, M. L.; Louie, S. G., et al. Graphene at the Edge: Stability and Dynamics. *Science* **2009**, 323, 1705-1708.
8. Bao, W.; Borys, N. J.; Ko, C.; Suh, J.; Fan, W.; Thron, A.; Zhang, Y.; Buyanin, A.; Zhang, J.; Cabrini, S., et al. Visualizing Nanoscale Excitonic Relaxation Properties of Disordered Edges and Grain Boundaries in Monolayer Molybdenum Disulfide. *Nat. Commun.* **2015**, 6, 7993.
9. Huang, Y. L.; Chen, Y.; Zhang, W.; Quek, S. Y.; Chen, C. H.; Li, L. J.; Hsu, W. T.; Chang, W. H.; Zheng, Y. J.; Chen, W., et al. Bandgap Tunability at Single-Layer Molybdenum Disulphide Grain Boundaries. *Nat. Commun.* **2015**, 6, 7298.
10. Bollinger, M. V.; Lauritsen, J. V.; Jacobsen, K. W.; Nørskov, J. K.; Helveg, S.; Besenbacher, F. One-Dimensional Metallic Edge States in MoS_2. *Phys. Rev. Lett.* **2001**, 87, 196803.
11. Karunadasa, H. I.; Montalvo, E.; Sun, Y. J.; Majda, M.; Long, J. R.; Chang, C. J. A Molecular MoS_2 Edge Site Mimic for Catalytic Hydrogen Generation. *Science* **2012**, 335, 698-702.
12. Jaramillo, T.; Jørgensen, K.; Bonde, J.; Nielsen, J.; Horch, S.; Chorkendorff, I. Identification of Active Edge Sites for Electrochemical H_2 Evolution from MoS_2 Nanocatalysts. *Science* **2007**, 317, 100.
13. Srivastava, A.; Sidler, M.; Allain, A. V.; Lembke, D. S.; Kis, A.; ImamoğluA. Optically Active Quantum Dots in Monolayer WSe_2. *Nat. Nanotechnol.* **2015**, 10, 491-496.
14. He, Y. M.; ClarkGenevieve; SchaibleyJohn, R.; He, Y.; ChenMing, C.; WeiYu, J.; DingXing; Zhang, Q.; Yao, W.; Xu, X., et al. Single Quantum Emitters in Monolayer Semiconductors. *Nat. Nanotechnol.* **2015**, 10, 497-502.
15. Chakraborty, C.; Kinnischtzke, L.; Goodfellow, K. M.; Beams, R.; Vamivakas, A. N. Voltage-Controlled Quantum Light from an Atomically Thin Semiconductor. *Nat. Nanotechnol.* **2015**, 10, 507-511.
16. KoperskiM; NogajewskiK; AroraA; CherkezV; MalletP; Veuillen, J. Y.; MarcusJ; KossackiP; PotemskiM. Single Photon Emitters in Exfoliated WSe_2 Structures. *Nat. Nanotechnol.* **2015**, 10, 503-506.
17. Zhang, C.; Johnson, A.; Hsu, C.-L.; Li, L.-J.; Shih, C.-K. Direct Imaging of Band Profile in Single Layer MoS_2 on Graphite: Quasiparticle Energy Gap, Metallic Edge States, and Edge Band Bending. *Nano Lett.* **2014**, 14, 2443-2447.
18. Wei, X.; Xiao, S.; Li, F.; Tang, D. M.; Chen, Q.; Bando, Y.; Golberg, D. Comparative Fracture Toughness of Multilayer Graphenes and Boronitrenes. *Nano Lett* **2015**, 15, 689-694.
19. Tao, J.; Shen, W.; Wu, S.; Liu, L.; Feng, Z.; Wang, C.; Hu, C.; Yao, P.; Zhang, H.; Pang, W., et al. Mechanical and Electrical Anisotropy of Few-Layer Black Phosphorus. *ACS Nano* **2015**, 9, 11362-11370.
20. Zhang, P.; Ma, L.; Fan, F.; Zeng, Z.; Peng, C.; Loya, P. E.; Liu, Z.; Gong, Y.; Zhang, J.; Zhang, X., et al. Fracture Toughness of Graphene. *Nat. Commun.* **2014**, 5, 3782.

21. Castellanos-Gomez, A.; Poot, M.; Steele, G. A.; van der Zant, H. S. J.; Agraït, N.; Rubio-Bollinger, G. Elastic Properties of Freely Suspended MoS_2 Nanosheets. *Adv. Mater.* **2012**, 24, 772-775.
22. Bertolazzi, S.; Brivio, J.; Kis, A. Stretching and Breaking of Ultrathin MoS_2. *ACS Nano* **2011**, 5, 9703-9709.
23. Lee, C.; Wei, X.; Kysar, J. W.; Hone, J. Measurement of the Elastic Properties and Intrinsic Strength of Monolayer Graphene. *Science* **2008**, 321, 385-388.
24. Yin, H.; Qi, H. J.; Fan, F.; Zhu, T.; Wang, B.; Wei, Y. Griffith Criterion for Brittle Fracture in Graphene. *Nano Lett.* **2015**, 15, 1918-1924.
25. Kim, K.; Artyukhov, V. I.; Regan, W.; Liu, Y.; Crommie, M. F.; Yakobson, B. I.; Zettl, A. Ripping Graphene: Preferred Directions. *Nano Lett.* **2012**, 12, 293-297.
26. Fujihara, M.; Inoue, R.; Kurita, R.; Taniuchi, T.; Motoyui, Y.; Shin, S.; Komori, F.; Maniwa, Y.; Shinohara, H.; Miyata, Y. Selective Formation of Zigzag Edges in Graphene Cracks. *ACS Nano* **2015**, 9, 9027-9033.
27. Das, S.; Gulotty, R.; Sumant, A. V.; Roelofs, A. All Two-Dimensional, Flexible, Transparent, and Thinnest Thin Film Transistor. *Nano Lett.* **2014**, 14, 2861-2866.
28. Akinwande, D.; Petrone, N.; Hone, J. Two-Dimensional Flexible Nanoelectronics. *Nat. Commun.* **2014**, 5, 5678.
29. Yuk, J. M.; Park, J.; Ercius, P.; Kim, K.; Hellebusch, D. J.; Crommie, M. F.; Lee, J. Y.; Zettl, A.; Alivisatos, A. P. High-Resolution Em of Colloidal Nanocrystal Growth Using Graphene Liquid Cells. *Science* **2012**, 336, 61-64.
30. Chen, C.; Lee, S.; Deshpande, V. V.; Lee, G.-H.; Lekas, M.; Shepard, K.; Hone, J. Graphene Mechanical Oscillators with Tunable Frequency. *Nat. Nanotechnol.* **2013**, 8, 923-927.
31. Conley, H. J.; Wang, B.; Ziegler, J. I.; Haglund, R. F.; Pantelides, S. T.; Bolotin, K. I. Bandgap Engineering of Strained Monolayer and Bilayer MoS_2. *Nano Lett.* **2013**, 13, 3626-3630.
32. Chenet, D. A.; Aslan, O. B.; Huang, P. Y.; Fan, C.; van der Zande, A. M.; Heinz, T. F.; Hone, J. C. In-Plane Anisotropy in Mono- and Few-Layer ReS_2 Probed by Raman Spectroscopy and Scanning Transmission Electron Microscopy. *Nano Lett.* **2015**, 15, 5667-5672.
33. Mishchenko, A.; Cao, Y.; Yu, G. L.; Woods, C. R.; Gorbachev, R. V.; Novoselov, K. S.; Geim, A. K.; Levitov, L. S. Nonlocal Response and Anamorphosis: The Case of Few-Layer Black Phosphorus. *Nano Lett* **2015**, 15, 6991-6995.
34. Muratore, C.; Varshney, V.; Gengler, J. J.; Hu, J. J.; Bultman, J. E.; Roy, A. K.; Farmer, B. L.; Voevodin, A. A. Thermal Anisotropy in Nano-Crystalline MoS_2 Thin Films. *Phys. Chem. Chem. Phys.* **2014**, 16, 1008-1014.
35. Ribeiro, H. B.; Pimenta, M. A.; de Matos, C. J. S.; Moreira, R. L.; Rodin, A. S.; Zapata, J. D.; de Souza, E. A. T.; Castro Neto, A. H. Unusual Angular Dependence of the Raman Response in Black Phosphorus. *ACS Nano* **2015**, 9, 4270-4276.
36. Wang, X.; Jones, A. M.; Seyler, K. L.; Tran, V.; Jia, Y.; Zhao, H.; Wang, H.; Yang, L.; Xu, X.; Xia, F. Highly Anisotropic and Robust Excitons in Monolayer Black Phosphorus. *Nat. Nanotechnol.* **2015**, 10, 517-521.
37. Wolverson, D.; Crampin, S.; Kazemi, A. S.; Ilie, A.; Bending, S. J. Raman Spectra of Monolayer, Few-Layer, and Bulk $ReSe_2$: An Anisotropic Layered Semiconductor. *ACS Nano* **2014**, 8, 11154-11164.
38. Wu, J.; Mao, N.; Xie, L.; Xu, H.; Zhang, J. Identifying the Crystalline Orientation of Black Phosphorus Using Angle-Resolved Polarized Raman Spectroscopy. *Angew. Chem. Int. Ed. Engl.* **2015**, 54, 2366-2369.
39. Wu, W.; Wang, L.; Li, Y.; Zhang, F.; Lin, L.; Niu, S.; Chenet, D.; Zhang, X.; Hao, Y.; Heinz, T. F., et al. Piezoelectricity of Single-Atomic-Layer MoS_2 for Energy Conversion and Piezotronics. *Nature* **2014**, 514, 470-474.
40. Xia, F.; Wang, H.; Jia, Y. Rediscovering Black Phosphorus as an Anisotropic Layered Material for Optoelectronics and Electronics. *Nat. Commun.* **2014**, 5, 4458.

41. Yamamoto, M.; Dutta, S.; Aikawa, S.; Nakaharai, S.; Wakabayashi, K.; Fuhrer, M. S.; Ueno, K.; Tsukagoshi, K. Self-Limiting Layer-by-Layer Oxidation of Atomically Thin WSe_2. *Nano Lett* **2015**, 15, 2067-2073.
42. Yamamoto, M.; Einstein, T. L.; Fuhrer, M. S.; Cullen, W. G. Anisotropic Etching of Atomically Thin MoS_2. *J. Phys. Chem. C* **2013**, 117, 25643-25649.
43. Zhang, S.; Yang, J.; Xu, R.; Wang, F.; Li, W.; Ghufran, M.; Zhang, Y.-W.; Yu, Z.; Zhang, G.; Qin, Q., et al. Extraordinary Photoluminescence and Strong Temperature/Angle-Dependent Raman Responses in Few-Layer Phosphorene. *ACS Nano* **2014**, 8, 9590-9596.
44. Liu, T. H.; Chen, Y. C.; Pao, C. W.; Chang, C. C. Anisotropic Thermal Conductivity of MoS_2 Nanoribbons: Chirality and Edge Effects. *Appl. Phys. Lett.* **2014**, 104, 5.
45. Kumar, N.; Najmaei, S.; Cui, Q.; Ceballos, F.; Ajayan, P. M.; Lou, J.; Zhao, H. Second Harmonic Microscopy of Monolayer MoS_2. *Phys. Rev. B* **2013**, 87, 161403.
46. Malard, L. M.; Alencar, T. V.; Barboza, A. P. M.; Mak, K. F.; de Paula, A. M. Observation of Intense Second Harmonic Generation from MoS_2 Atomic Crystals. *Phys. Rev. B* **2013**, 87, 201401.
47. Lin, Y.-C.; Komsa, H.-P.; Yeh, C.-H.; Björkman, T.; Liang, Z.-Y.; Ho, C.-H.; Huang, Y.-S.; Chiu, P.-W.; Krasheninnikov, A. V.; Suenaga, K. Single-Layer Res2: Two-Dimensional Semiconductor with Tunable in-Plane Anisotropy. *ACS Nano* **2015**, 9, 11249-11257.
48. Brivio, J.; Alexander, D. T. L.; Kis, A. Ripples and Layers in Ultrathin MoS_2 Membranes. *Nano Lett.* **2011**, 11, 5148-5153.
49. Jeong, H. Y.; Lee, S. Y.; Ly, T. H.; Han, G. H.; Kim, H.; Nam, H.; Jiong, Z.; Shin, B. G.; Yun, S. J.; Kim, J., et al. Visualizing Point Defects in Transition-Metal Dichalcogenides Using Optical Microscopy. *ACS Nano* **2016**, 10, 770-777.
50. Ly, T. H.; Chiu, M.-H.; Li, M.-Y.; Zhao, J.; Perello, D. J.; Cichocka, M. O.; Oh, H. M.; Chae, S. H.; Jeong, H. Y.; Yao, F., et al. Observing Grain Boundaries in Cvd-Grown Monolayer Transition Metal Dichalcogenides. *ACS Nano* **2014**, 8, 11401-11408.
51. Duong, D. L.; Han, G. H.; Lee, S. M.; Gunes, F.; Kim, E. S.; Kim, S. T.; Kim, H.; Ta, Q. H.; So, K. P.; Yoon, S. J., et al. Probing Graphene Grain Boundaries with Optical Microscopy. *Nature* **2012**, 490, 235-239.
52. Wengen, O.; Xin, Z. L.; Qunyang, L.; Yingying, Z.; Jiarui, Y.; Quan-shui, Z. Optical Methods for Determining Thicknesses of Few-Layer Graphene Flakes. *Nanotechn.* **2013**, 24, 505701.
53. Hoffman, T. B.; Clubine, B.; Zhang, Y.; Snow, K.; Edgar, J. H. Optimization of Ni–Cr Flux Growth for Hexagonal Boron Nitride Single Crystals. *J. Cryst. Growth* **2014**, 393, 114-118.
54. Du, K.-z.; Wang, X.-z.; Liu, Y.; Hu, P.; Utama, M. I. B.; Gan, C. K.; Xiong, Q.; Kloc, C. Weak Van Der Waals Stacking, Wide-Range Band Gap, and Raman Study on Ultrathin Layers of Metal Phosphorus Trichalcogenides. *ACS Nano* **2016**, 10, 1738-1743.
55. Zhao, Y.; Qiao, J.; Yu, P.; Hu, Z.; Lin, Z.; Lau, S. P.; Liu, Z.; Ji, W.; Chai, Y. Extraordinarily Strong Interlayer Interaction in 2D Layered PtS_2. *Adv. Mater.* **2016**, 28, 2399-2407.
56. Brec, R. Review on Structural and Chemical Properties of Transition Metal Phosphorous Trisulfides MPS_3. *Solid State Ionics* **1986**, 22, 3-30.
57. Griffith, A. A. The Phenomena of Rupture and Flow in Solids. *Philosophical transactions of the royal society of london. Series A, containing papers of a mathematical or physical character* **1921**, 221, 163-198.
58. Plimpton, S. Fast Parallel Algorithms for Short-Range Molecular-Dynamics. *J. Comput. Phys.* **1995**, 117, 1-19.
59. Jiang, J. W. Parametrization of Stillinger-Weber Potential Based on Valence Force Field Model: Application to Single-Layer MoS_2 and Black Phosphorus. *Nanotechn.* **2015**, 26, 315706.
60. Stukowski, A. Visualization and Analysis of Atomistic Simulation Data with Ovito-the Open Visualization Tool. *Model. Simul. Mater. Sc.* **2010**, 18, 015012.